Peer-reviewed version available at *Appl. Sci.* **2018**, *8*, 2059; doi:10.3390/app8112059

Review

A Review on Fault Current Limiting Devices to Enhance Fault Ride-through Capability of Doubly Fed Induction Generator Based Wind turbine

Seyed Behzad Naderi[1], Pooya Davari[2], Dao Zhou[2], Michael Negnevitsky[1], Frede Blaabjerg[2]

[1]School of Engineering and ICT, University of Tasmania, Hobart, TAS, Australia
[2]The Department of Energy Technology, Aalborg University, Aalborg, Denmark

*Correspondence: michael.negnevitsky@utas.edu.au; Tel.: +61 3 6226 7613

Abstract: The Doubly-Fed Induction Generator (DFIG) has significant features in comparison with Fixed Speed Wind Turbine (FSWT), which has popularized its application in power system. Due to partial rated back-to-back converters in the DFIG, Fault Ride-Through (FRT) capability improvement is one of the great subjects regarding new grid code requirements. To enhance the FRT capability of the DFIG, many studies have been carried out. Fault current limiting devices as one of the techniques are utilized to limit the current level and protect switches of the back-to-back converter from over-current damage. In this paper, a review is done based on fault current limiting characteristic of the proposed fault current limiting devices Therefore, Fault Current Limiters (FCLs) and Series Dynamic Braking Resistors (SDBRs) are mainly taken into account. Operation of all configurations including their advantages and disadvantages is explained. Impedance type and the fault current limiting devices' location are two important factors, which significantly affect the DFIG behaviour in the fault condition. These two factors are basically studied by the simulation and their effects on the key parameters of the DFIG are investigated. Finally, future works in respect to the FCL application in the FRT improvement of the DFIG have also been discussed.

Keywords: Wind power; Fault current limiters, Doubly-fed induction generator; Fixed speed wind turbine; Series dynamic braking resistor

1. Introduction

With a high penetration level of Wind Energy Conversion Systems (WECS) in the grid, the power system operators encounter new challenging issues, which could affect the stability of the power system. Therefore, keeping the wind turbines connected to the grid during faults with a high wind power penetration is literally important, which is known as Fault Ride-Through (FRT) capability [1]. Due to many significant characteristics of Doubly-Fed Induction Generator (DFIG) based wind turbines, they are widely employed in the power system especially for the multi-MW applications [2]. In the configuration of the DFIG, the stator of the DFIG is directly connected to the grid and the rotor circuit is linked to the network by partial scale back-to-back voltage source converters. During the fault condition, transient over-current goes through the rotor circuit towards the Rotor Side Converter (RSC). The rotor over-current can either trip out the DFIG or damage the power electronic devices [3]. Therefore, keeping the DFIG based wind turbine connected to the utility and preventing the equipment from damage are important during the fault. It is clear that, for secure power system operation, the wind turbines should meet the grid requirements. Fig. 1(a) presents the grid code requirement for different countries for the FRT of the wind turbine [4]. In the lower area of each curve,

the wind turbine could be disconnected, but for any point in the upper area, the wind turbine should remain connected to the power system. The FRT requirement varies from countries following characteristics of the power system. Among the different grid codes, which are regulated by the various operators, the "*E.ON*" grid code has the most severe FRT requirements [1, 5]. The "*E.ON*" grid code is illustrated with more details in Fig. 1(b). With regard to "*E.ON*", even if the Point of the Common Coupling (PCC) voltage drops to zero for 150 ms after the fault occurrence, the wind turbine must not be disconnected from the grid.

In the literature, different methods have been studied to enhance the FRT capability of the DFIG [6]. The previous introduced approaches can be classified as crowbar (active and passive) [7, 8], DC braking chopper [9], new configurations for the DFIG [10, 11], the advanced control techniques in back-to-back voltage source converters [12] and also adding new hardware in the DFIG.

As adding new hardware in the DFIG, one of the common techniques is to employ fault current limiting devices to improve the FRT capability of the DFIG. Fault Current Limiters (FCLs) and Series Dynamic Braking Resistors (SDBRs) are placed in series connection of different locations in the DFIG (the stator side, the terminal, the DC link between the RSC and the DC link capacitor and the rotor side). In this paper, a review of most existing literature, which investigates the fault current limitation in the DFIG, are done. To improve the FRT capability of the DFIG, different configurations of the FCLs have been employed. Fig. 2 shows the diagram of all employed FCLs to enhance the FRT capability of the DFIG. The operational behaviour of each configuration is briefly discussed in normal and fault condition. The FCL structure can be categorized in respect to their impedance type during the fault condition. In the simulation section, the impedance type and the FCL's location will be discussed, which have various impacts on the key parameters of the DFIG. In this paper, the detailed operation of the configurations is not taken into account and only the functionality is considered. In fact, steady state of the fault condition is discussed, which almost depends on the type and size of the impedance in the fault current limiting devices.

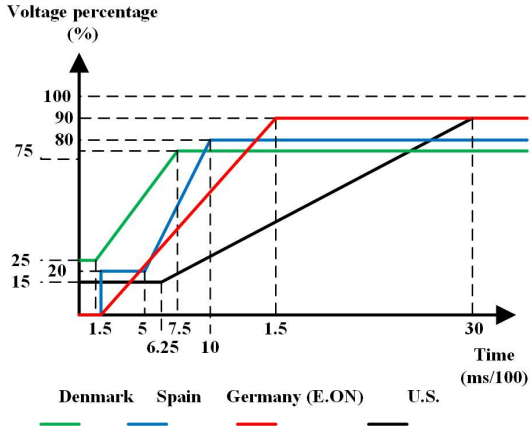

Fig. 1(a). The grid code requirement for the fault ride through of the wind turbine in the different countries [4].

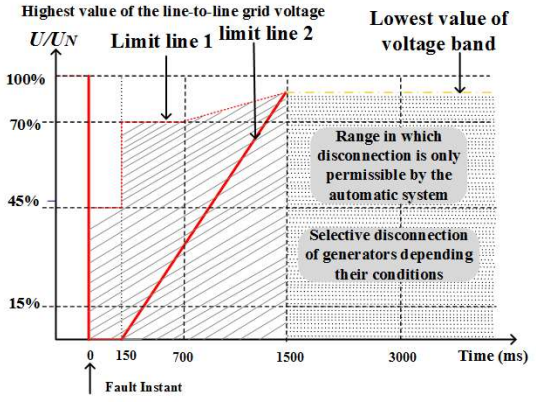

Fig. 1(b). Limits curves for the fault ride through requirement of the "*E.ON*" grid code [5].

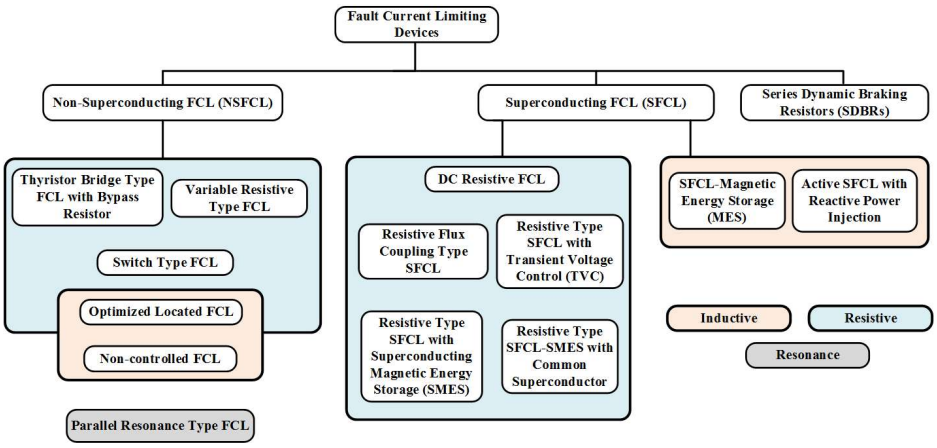

Fig. 2. Diagram of the Fault Ride Through (FRT) capability enhancement by fault current limiting devices in the doubly fed induction generator.

In the following, the operation of the DFIG is briefly expressed with the RSC's and Grid Side Converter (GSC)'s control circuits. In section III, other approaches are mentioned with their pros and cons. In section IV, an overview of almost all fault current limiting devices is studied with their configuration and the behaviour in normal and the fault conditions. Section V, which is the simulation section, shows how the impedance and the location of the fault current limiting devices affect the DFIG operation in steady state of the fault condition. Furthermore, a discussion is raised on the simulation results. Finally, a conclusion is given.

2. Doubly Fed Induction Generator

The configuration of the DFIG is shown in Fig. 3(a). During the fault condition, a very high electromotive force (EMF) is induced in the rotor due to electromagnetic interaction with the stator and the rotor of the DFIG, which leads to over-voltage and over-current in the rotor side. The over-voltage and the over-current could damage the RSC components if the semiconductor switches are continuously trigged in the fault condition. In this situation, the rotor high transient over-current passes through the switches.

Meanwhile, the excess active power, which is not able to be delivered to the power system in the fault condition, charges the DC link capacitor and rapidly increase the DC link voltage. So, with regard to Fig. 3(a), the DC braking chopper typically operates to dissipate the excess energy and keep the DC link voltage (V_{DC}) in a constant value. It should be noticed that because of operation of the DC braking chopper and time-varying characteristics of electromagnetic interaction with the stator and the rotor, the response of the DFIG is very non-linear. However, during the fault, the DC link voltage is almost kept constant when the DC braking chopper operates. In a static stator-oriented reference frame, the rotor and the stator fluxes, $\vec{\psi}_r$, $\vec{\psi}_s$, and the rotor and the stator voltages, $\vec{v}_r$, $\vec{v}_s$, are expressed as follows with respect to Park model of the DFIG [13]:

$$\vec{v}_s = R_s\vec{i}_s + \frac{d\vec{\psi}_s}{dt} \tag{1}$$

$$\vec{v}_r = R_r\vec{i}_r + \frac{d\vec{\psi}_r}{dt} - j\omega_r\vec{\psi}_r \tag{2}$$

$$\vec{\psi}_s = L_s\vec{i}_s + L_m\vec{i}_r \tag{3}$$

$$\vec{\psi}_r = L_m\vec{i}_s + L_r\vec{i}_r \tag{4}$$

whereby $\vec{i}$, ω, R, and L represent current, angular frequency, resistance and inductance, respectively. Also, stator, mutual and rotor parameters are mentioned by subscripts of s, m and r, respectively. By means of (3) and (4), $\vec{\psi}_r$ is computed with respect to $\vec{i}_r$ and $\vec{\psi}_s$. (5) expresses $\vec{\psi}_r$ as follows:

$$\begin{cases} \vec{\psi}_r = \dfrac{L_m \vec{\psi}_s}{L_s} + \sigma L_r \vec{i}_r \\ \sigma = 1 - \dfrac{L_m^2}{L_s L_r} \end{cases} \tag{5}$$

whereby the leakage coefficient is represented by σ. To calculate the rotor voltage with respect to (2) and (5), the following expression is deduced:

$$\vec{v}_r = \overbrace{\frac{L_m}{L_s}\left(\frac{d}{dt} - j\omega_r\right)\vec{\psi}_s}^{\vec{v}_{ro}} + \left(R_r + \sigma L_r\left(\frac{d}{dt} - j\omega_r\right)\right)\vec{i}_r \tag{6}$$

whereby $\vec{v}_{ro}$ denotes the rotor voltage when the rotor is an open circuit condition and the rotor current is zero. If the reference frame is changed from a static stator-oriented reference frame to a rotor-oriented reference frame, the rotor voltage is expressed in (7).

$$\vec{v}_r^r = \vec{v}_{ro}^r + \left(R_r + \sigma L_r \frac{d}{dt}\right)\vec{i}_r^r \tag{7}$$

whereby $\vec{v}_r^r$, $\vec{v}_{ro}^r$ and $\vec{i}_r^r$ are the rotor voltage, the open circuit rotor voltage and the rotor current in the rotor-oriented reference frame. With regard to (7), the rotor side electrical circuit is modelled by a three-phase voltage source of $\vec{v}_{ro}^r$, the rotor resistance (R_r) and the transient inductance (σL_r) during the fault condition. The level of rotor transient over-current will be changed with regard to the fault instant, the type of fault and the voltage sag depth [14]. For instance, during a symmetrical grid fault, the open circuit rotor voltage $\vec{v}_{ro}^r$ includes two expressions as follows:

$$\vec{v}_{ro}^r = (1-p)V_s \frac{L_m}{L_s} s e^{js\omega_s t} - \frac{L_m}{L_s}\left(\frac{1}{\tau_s} + j\omega_r\right)\frac{pV_s}{j\omega_s} e^{-j\omega_r t} e^{-t/\tau_s} \tag{8}$$

whereby the pre-fault stator voltage magnitude, the voltage sag depth and the slip are represented by V_s, p and s during the symmetrical grid fault, respectively. Also, τ_s decaying time constant is equal to L_s/R_s.

The schematic of control circuits for the rotor side converter and the grid side converter are presented in Fig. 3(b) [15]. In both control systems, PI controllers are employed for regulation. In the rotor side converter, the reference active power P_{ref} is computed in respect to Maximum Power Point Tracking (MPPT) and then the extracted active power $P_{extract}$, which depends on the wind speed, is compared to P_{ref}. Consequently, the d-axis reference current of rotor is achieved. Meanwhile, the reference value for the reactive power of the stator $Q_{s\text{-}ref}$ is considered zero. Therefore, during the normal operation, the absorbed reactive power Q_s from the stator side of the DFIG will be equal to the reference value and the required reactive power for the DFIG will be covered by the back-to-back converters. To maintain the DC link voltage in constant value, the grid side converter provides the active power to the rotor side. Therefore, the d-axis reference current is obtained by comparing the DC link voltage with the reference value, $V_{DC\text{-}ref}$. Meanwhile, the reactive power, Q, in the GSC and the RSC is adjusted by the reference value of Q_{ref}.

Preprints (www.preprints.org) | NOT PEER-REVIEWED | Posted: 27 September 2018 doi:10.20944/preprints201809.0538.v1

Peer-reviewed version available at Appl. Sci. 2018, 8, 2059; doi:10.3390/app8112059

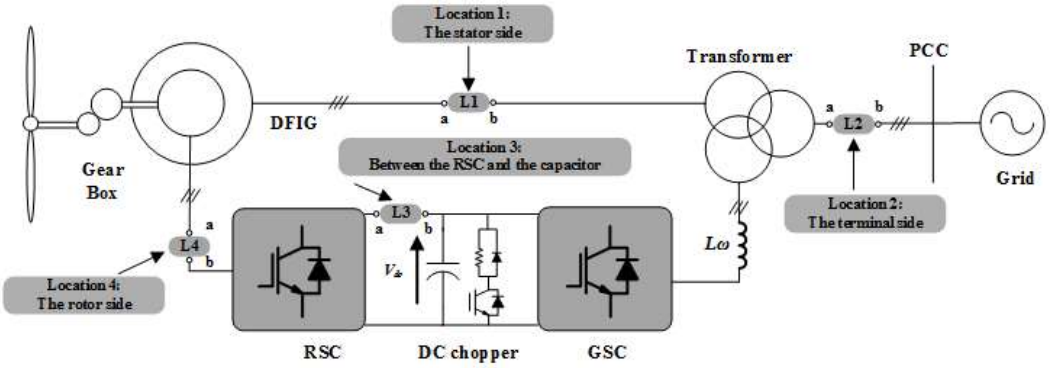

Fig. 3(a). The doubly fed induction generator configuration with all possible highlighted locations for the fault current limiters and series dynamic braking resistors in the fault ride through capability improvement.

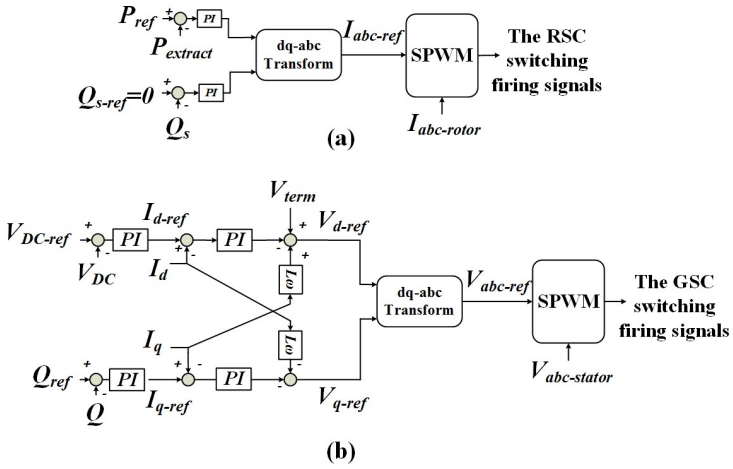

Fig. 3(b). The schematic of control circuits for (a) the rotor side converter and (b) the grid side converter.

3. Fault Ride-Through

As mentioned in the Introduction, there are different methods to improve the FRT capability of the DFIG. Advanced control methods are discussed mostly in the papers. These methods control active and reactive power injections of the DFIG to restore the PCC voltage during the fault. Most of these methods are complicated and they are not so interesting for the industry [16]. Furthermore, during the zero voltage sag in the PCC, the terminal voltage as a reference will be lost and the control method might be inapplicable [17].

Another method is to change the configuration of the DFIG. In this situation, the changes happen in the back-to-back converters. A fault tolerant DFIG based wind turbine has been proposed to enhance the FRT capability [10, 18]. The configuration of the proposed DFIG is shown in Fig. 4. Instead of utilizing general six semiconductor switch converter, a nine-switch GSC has been used. In normal operation, three lower switches are in the on state. When a fault occurs, three lower switches operate to compensate the voltage on the neutral side of the winding in the stator. Another changing in the configuration of conventional DFIG has been studied in [11, 19]. The proposed scheme is shown in Fig. 4 with gray colour. Similar to the conventional DFIG, the stator is directly linked to the gird through the terminal. However, an extra converter, which is connected to the star point of the stator winding, is employed to provide an effective active power transfer to the grid and a better power system disturbance ride through during the low voltage. As it is clear from Fig. 4, these changes in

Peer-reviewed version available at Appl. Sci. 2018, 8, 2059; doi:10.3390/app8112059

the configuration of the conventional DFIG are not probably of interest to industry. However, to be practically implemented, they should have economical justification.

Adding extra hardware is another scheme to improve the FRT capability of the DFIG. Crowbar protection, DC braking chopper, voltage sag compensation devices and fault current limiting devices are employed as extra hardware in the DFIG to enhance the ride-through capability during the fault condition. The crowbar protection is the most well-known scheme, which is practically employed and utilized in the FRT improvement of the DFIG. The configuration of the crowbar is shown in Fig. 4. The crowbar includes a three-phase diode bridge rectifier, a bypass resistance and a switch, either a semiconductor switch such as Isolated Gate Bipolar Transistor (IGBT) in the active crowbar or a switch such as a thyristor in the conventional crowbar. The active crowbar has been introduced to overcome continuous absorption of the reactive power by Squirrel Cage Induction Generator (SCIG) in the conventional crowbar [7]. To operate the active crowbar by a semiconductor switch and cease the RSC switching, a threshold current or a threshold voltage is defined regarding the transient over-current in the rotor side or the over-voltage in the DC link, respectively. Whenever the measured current voltage is less than the threshold current voltage, the DFIG converters resume to normal operation [8]. The RSC stop and the reactive power absorption by the active crowbar are the main disadvantages of this method.

DC braking chopper is another scheme to keep the DC link voltage value in the safe area of operation during the fault condition. The schematic of the DC chopper is depicted in Fig. 4. The parallel connected configuration of the DC chopper consists of a resistor in series with a semiconductor switch. An anti-parallel diode is also utilized to protect the chopper switch from voltage spike when the semiconductor switch goes to the off state. However, the DC braking chopper does not effectively restrict the rotor transient over-current. Therefore, high rated anti-parallel diodes should be employed in the RSC [9]. Similar to the crowbar scheme, when the DC chopper is activated, the RSC switching is ceased.

A Static Synchronous Compensator (STATCOM) as the voltage sag compensation device has been discussed in [20]. Fig. 4 shows the location and simple configuration of the STATCOM. Due to the low capacity of back-to-back converters, in case of the fault in the weak utility, there is a possibility of a voltage instability. Then, the voltage sag compensation devices such as the STATCOM has been proposed to support the voltage profile during the fault condition. There are coordinated and independent reactive power controls between the STATCOM and the DFIG [20, 21]. In the independent control method, the voltage control is only done by the STATCOM. The STATCOM should incorporate with a fault current limiting method as it is not solely able to restrict the fault current level in the RSC. Also, Dynamic Voltage Restorers (DVR) is another voltage sag compensation device, which have been utilized to overcome voltage sag during the fault. In Fig. 4, the simple configuration of the DVR is presented. Similar to the STATCOM, auxiliary methods should incorporate to the DVR like changing the control method of the back-to-back converters or pitch angle control [22]. It should be noticed that these mentioned devices require large storage capacity and a high number of semiconductor switches.

From a fault current limiting point of view, the FCLs and the SDBRs are employed to restrict the fault current level in the DFIG. Up until now, many configurations of FCLs have been proposed and studied. The FCL structures can be divided into two categories with regard to impedance type and components. Considering the impedance type, they are resistive, inductive, resistive-inductive and resonance type FCLs. Meanwhile, whether superconductor utilized or not, there is another category

[23]. Recently, a new approach of applying the FCLs has been proposed with the capability of producing variable resistance [24]. Considering the component type, the FCLs are either solid state or saturated core transformer [14]. Despite of the current limiting characteristics of the FCLs, they have been employed for different applications. From a transient stability point of view, the application of variable and controllable resistance FCLs has been proved [24]. Regarding the location of the FCLs, they are also employed to compensate the voltage sag in the PCC [25].

In order to improve the FRT capability of the DFIG, the FCLs are placed in different locations of the DFIG. Fig. 3(a) shows the studied locations in the literature. In each location with respect to the FCL impedance type, the impacts on the key parameters of the DFIG are different during the fault condition. From the FCL's location point of view, the FCLs are mostly located at the terminal side and the stator side of the DFIG. Some of the FCLs are placed in the rotor side and a few of the configurations are in the DC link. Meanwhile, from an impedance point of view, the FCLs are mostly the resistive type as it is clear from Fig. 2. In the following section, it will be discussed how the impedance type and the FCL's location could affect the FRT capability of the DFIG based wind turbine. It will be also mentioned at which location and which impedance type could be a best choice to have the favourite FRT capability of the DFIG. In the following section, the FCLs' structure are categorized based on the impedance type.

4. Fault Current Limiting Devices

As mentioned, the FCLs and the SDBRs are employed as the fault current limiting devices to enhance the FRT capability of the DFIGs. At first, different structures of the FCLs and SDBRs are studied regarding the impedance type of each configuration and then a comparison will finally be done.

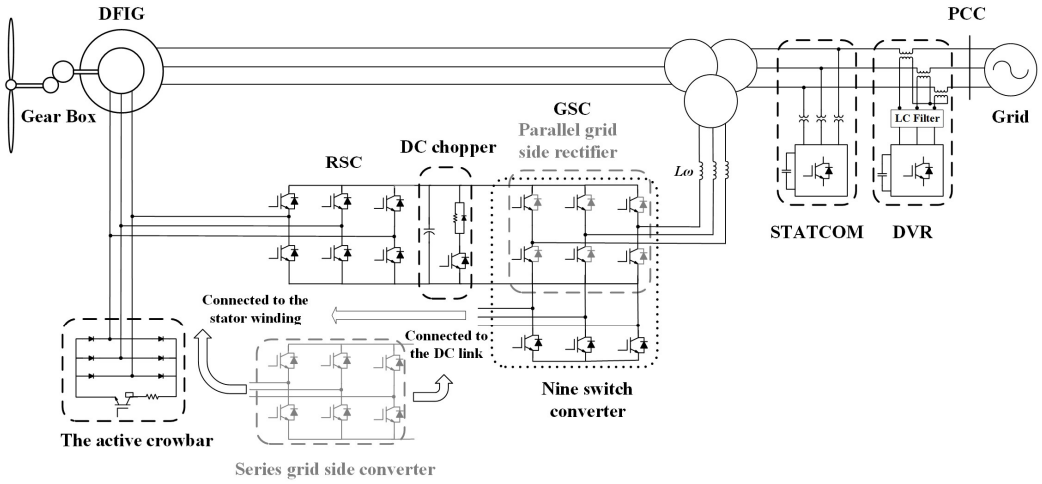

Fig. 4. The DFIG configuration with the most well-known FRT enhancement approaches.

4.1. Non-Superconducting FCL

4.1.1 Inductive type FCL: Non-controlled FCL

In [26], A cost-effective topology of a non-controlled FCL to improve the FRT capability of DFIG has been studied. The non-controlled FCL is placed in the rotor side, which is shown in Fig. 5(a). Its configuration is similar to a three-phase bridge type FCL. The limiting inductance is non-

Preprints (www.preprints.org) | NOT PEER-REVIEWED | Posted: 27 September 2018 doi:10.20944/preprints201809.0538.v1

Peer-reviewed version available at Appl. Sci. 2018, 8, 2059; doi:10.3390/app8112059

superconductor, which is cost-effective from an industrial point of view. Regarding the location of the FCL, inserting the SC either in the stator side or in the rotor side has different impacts. When the non-controlled FCL is located in the stator side, regarding (9) and (10), the value of back EMF voltage and the transient inductance of the rotor are changed as follows:

$$\vec{V}_{0r} = \frac{L_m}{L_s + a^2 L_{FCL}} \frac{d\vec{\psi}_s}{dt} \tag{9}$$

$$\sigma_{L1-FC} = 1 - \frac{L_m^2}{(L_s + a^2 L_{FCL}) L_r} \tag{10}$$

Fig. 5(b) shows the variation of the leakage coefficient by changing the FCL's impedance. As it is clear by (9), by increasing the inductance of the FCL in the stator side, the value of rotor back EMF voltage decreases. Therefore, the RSC has a good controllability to counteract the stator flux oscillations. However, absolute value of the leakage coefficient significantly decreases and damps by increasing the FCL's inductive impedance. In fact, there is the possibility that the rotor transient over-current is not restricted to an acceptable range. It should be mentioned that by locating the FCL in the stator side, the stator voltage is resumed to some extent. By placing the FCL in the rotor side, the leakage coefficient is expressed as follows:

$$\sigma_{L4-FCL} = 1 - \frac{L_m^2 - a^2 L_{FCL} L_s}{L_s L_r} \tag{11}$$

When the inductive FCL is located in the rotor side, the variation of the leakage coefficient is also shown in Fig. 5(b). In order to find out the variation of the leakage coefficient, some points should be taken into account. For the inductive impedance of the FCL located in the rotor side, any impedance value lower or higher than the intersection point of curves could result in good rotor transient over-current limitation. Otherwise, the FCL could have inverse impact in limiting the rotor transient over-current. As a result, if the inductive FCL is going to be located in the rotor side, its impedance should be lower or higher and far away than from the intersection point of the curves in order to get good current limitation capability. However, it should be noticed that from limiting the rotor transient over-current point of view, the inductive FCL in the rotor side is more effective than placing the FCL in the stator side. Furthermore, it should be noticed that the rotor back EMF voltage remains unchanged and consequently a rather high electromagnetic torque oscillation might happen due to the weak controllability of the RSC on the stator flux linkage. In addition, there is not any possibility to restore the stator voltage.

4.1.2 Inductive-resistive type FCL Optimized located FCL

An optimized located FCL has been proposed in [27], and it is shown in Fig. 6. The proposed FCL has been placed in the DC link of the DFIG. However, the RSC's switches are turned off during the fault condition and high-level fault currents should pass through the high rated anti-parallel diodes. The FCL is resistive and is capable to limit the fault current only in one direction. The FCLs' resistance is bypassed by a semiconductor switch during normal condition. To protect the semiconductor switches from over-voltage, a surge arrestor is connected in parallel with each switch of the FCL. It should be noted that the optimized located FCLs can cause over-voltage on the RSC switches during the switching in normal operation. To avoid this destroying voltage, auxiliary circuits should be applied, which result in high cost and large size.

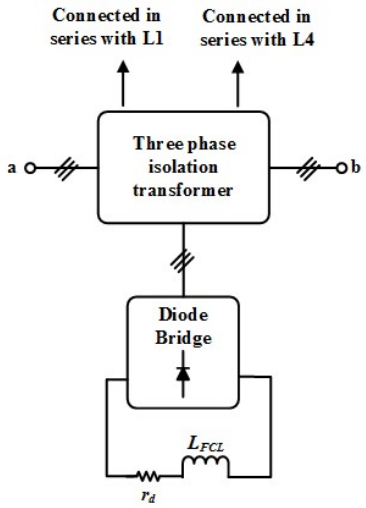

Fig. 5(a). The non-controlled inductive fault current limiter.

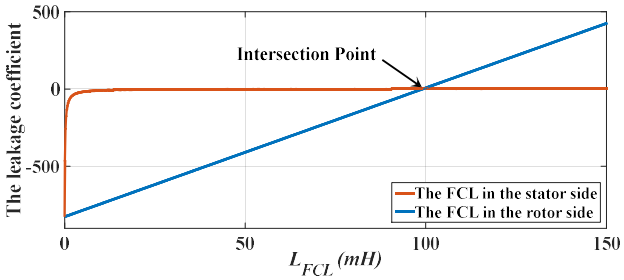

Fig. 5(b). The leakage coefficient variation with the FCL inductance variation in the stator and the rotor sides.

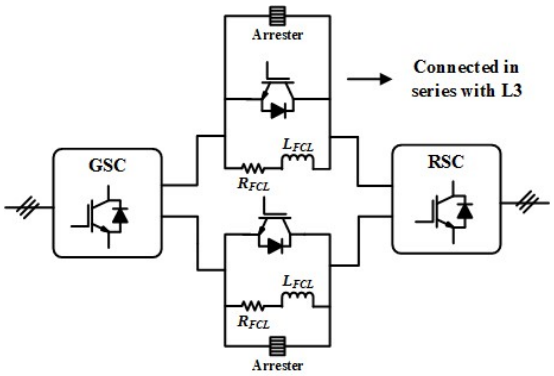

Fig. 6. The optimized located FCL.

4.1.3 Resistive Type FCL: Thyristor bridge type FCL

A thyristor Bridge Type FCL with Bypass Resistor (BTFCL-BR) is presented in [28]. Fig. 7 shows the BTFCL-BR. In [28], the stator side location has only been studied. The main advantage of the BFCL-BR is not to use the SC. Because of employing Non-Superconductor (NSC), there are high voltage spikes on the NSC, which affect the stator voltage and consequently generate severe stator flux and electromagnetic torque oscillations during normal operation. Therefore, the Bypass Resistor (BR) has been proposed not only to restrict the high voltage spikes but also eliminate the most current harmonics in normal operation of the power system. During the fault condition, after fault detection, the thyristors signal triggering will go to the off state. So before turning off the thyristors in the zero-current crossing, the bypass resistor and the NSC restricts the stator fault currents in first instances of the fault. After going to the off state of all thyristors, the bypass resistance solely limits the stator fault current. Increasing the resistance in the stator side decreases the time constant of the stator current and meanwhile restricts the stator fault current in a good manner. From the number of thyristor switches point of view, it can be a disadvantage for this configuration.

Preprints (www.preprints.org) | NOT PEER-REVIEWED | Posted: 27 September 2018 doi:10.20944/preprints201809.0538.v1

Peer-reviewed version available at Appl. Sci. 2018, 8, 2059; doi:10.3390/app8112059

4.1.4 Resistive type FCL: Switch type FCL (STFCL)

A Switch Type FCL (STFCL) has been proposed in [14], and it is shown in Fig. 7(b). The difference of the STFCL compared to the BTFCL is to use an inductor as a fault-current-limiting impedance instead of the BR. Furthermore, instead of using thyristor-bridge, a diode bridge has been employed in the STFCL. A snubber circuit has been used in order to utilize the inductor to suppress the transient over-voltage on the semiconductor switch, when it goes to the off state after the fault detection. After suppressing the first spikes by C_f, which is smaller than C_a, C_a absorbs the excess energy in the stator up until its voltage reaches to steady state. Afterwards, the current pass in the DC side of the diode bridge is blocked and the inductor does its limiting operation. The STFCL impacts on the DFIG are the same as discussed for the non-controlled FCL, when it is located in the stator side.

4.1.5 Resistive type FCL: Variable resistive type FCL

In [29], a Variable Resistive Type FCL (VR-FCL) has been placed in the PCC to improve the transient stability of a hybrid power system composed of the DFIG, a Photovoltaic (PV) plant, and a Synchronous Generator (SG). The configuration of the VR-FCL is similar to [30] and shown in Fig. 8(a). However, to make better transient stability improvement, the pre-fault conditions including pre-fault active power of the hybrid generation units and fault location have been taken into account. Regarding the pre-fault conditions, to control the VR, three nonlinear controller schemes including Fuzzy Logic Controller (FLC), Static Nonlinear Controller (SNC), and an Adaptive-Network-based Fuzzy Inference System (ANFIS) have been discussed. The operation of ANFIS-based VR-FCL is better than the FLC and the FLC better than the SNC. The factors to evaluate the operation of each controller are the rotor speed deviation of the DFIG, the DC link voltage deviation of the PV generator, and the load angle deviation of the SG. The concept of the pre-fault conditions to get the maximum transient stability has been previously proposed in [30]. However, it should be noticed that the dynamic behaviour of the DFIG is completely different than the other generation units [13]. As soon as the fault happens especially three-phase fault, due to the exponential current variation in the stator of the DFIG, the voltage drop on the FCL cannot be enough particularly after damping the stator current in first cycles of power system frequency.

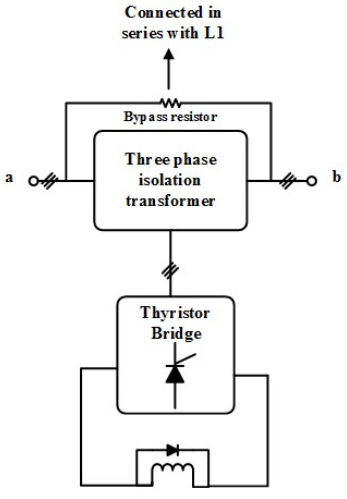

Fig. 7(a). The thyristor Bridge Type Fault Current Limiter with Bypass Resistor (BTFCL-BR).

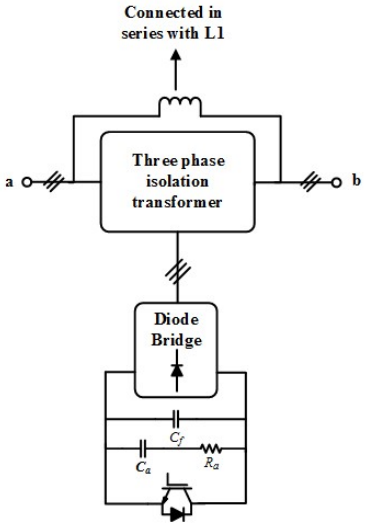

Fig. 7(b). The Switch Type Fault Current Limiter (STFCL) with a snubber circuit.

4.1.6 Resonance Type FCL: Parallel resonance type FCL

In [31], as shown in Fig. 8(b), a parallel resonance type FCL has been investigated and compared to the bridge type FCL with parallel resistive-inductive shunt impedance. The idea of parallel resonance type FCL has been proposed in [32]. In normal operation, the semiconductor switch is in the on state and the parallel resonance is bypassed. After a fault occurrence, the semiconductor switch goes to the off state. So, the fault current passes through the parallel impedance and is limited by the resonance type FCL which helps to enhance the FRT capability of the DFIG. Considering the assessment factors including the deviation of the wind farm terminal voltage, active power of the wind farm and rotor speed of the DFIG, the parallel resonance type FCL has better operation in compassion with the bridge type FCL with parallel resistive-inductive shunt impedance.

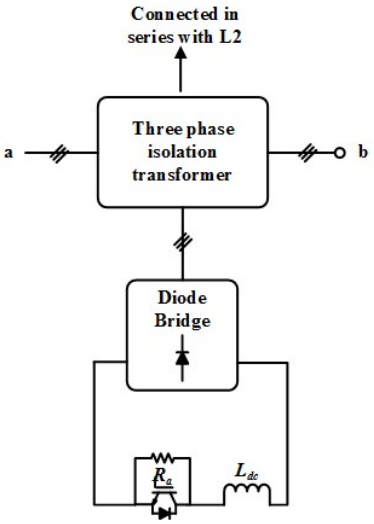

Fig. 8(a). The Variable Resistive Type Fault Current Limiter (VR-FCL).

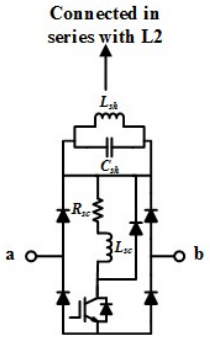

Fig. 8(b). The parallel resonance type fault current limiter.

4.2. Superconducting FCL

4.2.1 Inductive Type FCL: Superconducting Fault Current Limiter–Magnetic Energy Storage System (SFCL-MES)

Although, the superconducting FCLs are not of interest for industry from an economical point of view [28], so many configurations have been proposed to employ the superconductor in the FRT capability improvement of the DFIG. A Superconducting Fault Current Limiter–Magnetic Energy Storage System (SFCL-MES) has been presented in [33, 34]. Its configuration is shown in Fig. 9(a). The SFCL-MES can smooth the active power fluctuations and stabilize the DC link voltage together with limiting the fault current. The SFCL has been studied in both the rotor side and the stator side. The SFCL-MES is able to control the superconductor (SC) stored energy and the output power of the DFIG. As it is discussed, placing the inductive FCL either at the stator side or at the rotor side has different impacts. By locating the inductive FCL at the stator side, the stator flux oscillations are limited by decreasing the rotor back EMF. However, as mentioned before, the rotor transient over-current is not probably restricted well with the inductive FCL in the stator side than when the inductive FCL is placed in the rotor side. In fact, locating the inductive type FCL in the rotor side

increases the leakage coefficient more than when the FCL is placed in the stator side. However, it may decrease the RSC controllability due to the unchanged rotor back EMF voltage.

4.2.2 Inductive Type FCL: Active SFCL with Reactive Power Injection

An active SFCL to compensate the voltage sag in the PCC and restrict the fault current level has been studied in [35], and shown in Fig. 9(b). An air-core superconductive transformer is placed in series connection of the terminal of the DFIG. A three-phase converter with split DC link capacitors has been connected to the secondary side of the transformer. The converter injects a controlled value of the current to compensate the voltage drop on the PCC during the fault condition and surpass the current level. However, in this configuration, the cost of the superconductor and converter should be taken into account.

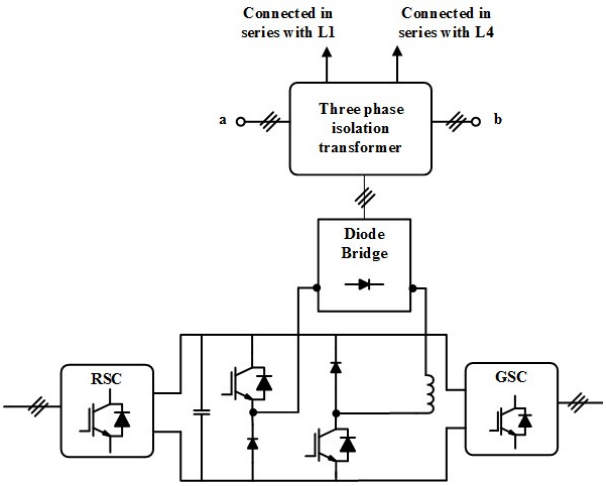

Fig. 9(a). The Superconducting Fault Current Limiter–Magnetic Energy Storage System (SFCL-MES).

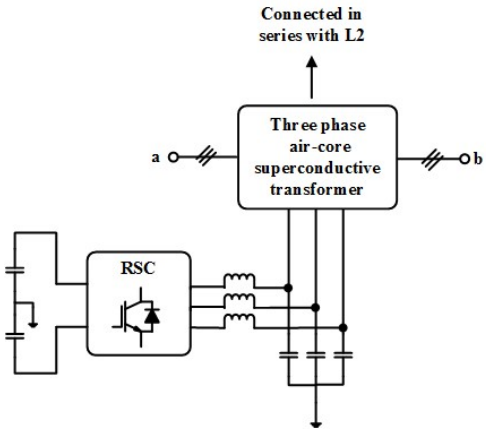

Fig. 9(b). The active superconducting fault current limiter.

4.2.3 Resistive Type FCL: DC resistive SFCL

In [36] and [37], a DC resistive Superconducting FCL (SFCL) (Fig. 10(a)) is placed in the PCC to limit the fault current level. There is not any novelty both in the configuration and the control part of the FCL. Meanwhile, as mentioned, using the SC increases the installation cost of the structure. In fact, the commercial application of the SFCL might be unavailable due to high cost.

4.2.4 Resistive Type FCL: Resistive-flux-coupling-type SFCL

A resistive-flux-coupling-type SFCL has been proposed in [38], and is shown in Fig. 10(b). The SFCL is composed of a coupling transformer, a Superconductor (SC) and a semiconductor switch (S1). Furthermore, an arrestor is employed to overcome the overvoltage in switching instances. In normal operation, S_1 is closed and if the coupling coefficient is supposed to be one, then the FCL's impedance is almost zero. When the fault happens, S_1 goes to the off state, and the overvoltage is restricted by the arrestor. The SC enters to the fault current pass to limit the current level. It should be noticed that placing a resistive impedance in the stator side can be much more effective than in the rotor side due to the voltage sag compensation and much more excess active power absorption. The resistive type FCL in the stator side limits both the stator and rotor currents effectively.

Peer-reviewed version available at Appl. Sci. 2018, 8, 2059; doi:10.3390/app8112059

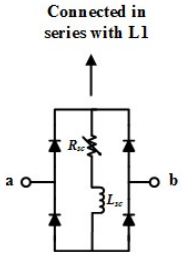

Fig. 10(a). The DC resistive superconducting fault current limiter.

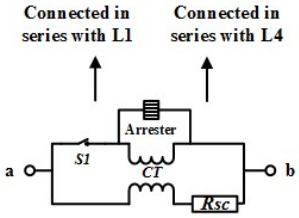

Fig. 10(b). The resistive-flux-coupling-type SFCL.

4.2.5 Resistive Type FCL: Resistive type SFCL with Transient Voltage Control (TVC)

Different configurations of the resistive type SFCL have been placed at the terminal of the DFIG. A cooperative FRT improvement by the resistive type SFCL with Transient Voltage Control (TVC) by the DFIG converters has been studied in [39]. It has been mentioned that the voltage sag compensation by TVC or fault current limiting characteristics of the SFCL cannot solely improve the PCC voltage during the fault condition. To some extent post-fault voltage sag compensation in the PCC by the SFCL as a passive voltage compensator results in much more reactive power injection by the converters as an active voltage compensator.

4.2.6 Resistive Type FCL: Superconducting Magnetic Energy Storage (SMES) with the SFCL

In [40], instead of employing the TVC in the converters, a Superconducting Magnetic Energy Storage (SMES) has been applied together the SFCL, and is presented in Fig. 11(a). The main application of the SMES is to smooth the active power fluctuation after the fault current limiting by the SFCL. However, in [39], it has been noted that the SFCL is not solely able to effectively improve the PCC voltage.

In [41], the authors of [40] made an improvement in the configuration of the SFCL-SMES. Instead of using two separate SCs, one in the SFCL and another in the SMES, one common SC has been employed in two DC choppers, as shown in Fig. 11(b). During fault condition, the DC chopper related to the FCL enters to the fault current path. After fault removal, the DC chopper of the SMES operates and the remaining active power fluctuations are restricted as discussed in [40].

4.2.7 Resistive Type FCL: Resistive type SFCL in the rotor side

In addition to place the resistive type SFCL in the terminal of the DFIG, different configurations have been located in the rotor side. In [42, 43], the proposed resistive type SFCL in the rotor side has the effective operation in limiting the rotor transient over-current. Meanwhile, due to active power consumption in the rotor side, the DC link over-voltage is avoided. However, the RSC controllability gets worse in practice as mentioned before. Although, the voltage dip in the PCC has been improved by the SFCL in the rotor side, the SFCL in the stator side either inductive or resistive has a better performance for the voltage sag compensation compared to the rotor side.

In [44], a resistive solid state FCL has been studied in the rotor side. The FCL is composed of antiparallel semiconductor switches, which are employed to bypass or insert the resistance. The FCL operates as a passive compensator to aid the converters as an active compensator as also discussed in [40].

Preprints (www.preprints.org) | NOT PEER-REVIEWED | Posted: 27 September 2018 doi:10.20944/preprints201809.0538.v1

Peer-reviewed version available at Appl. Sci. 2018, 8, 2059; doi:10.3390/app8112059

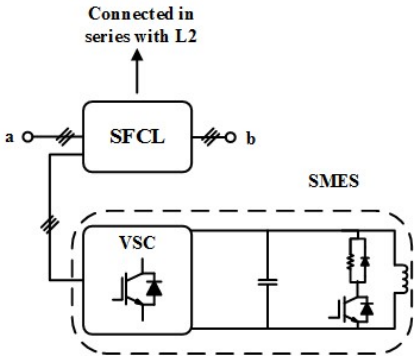

Fig. 11(a). The Superconducting Magnetic Energy Storage (SMES) together the SFCL.

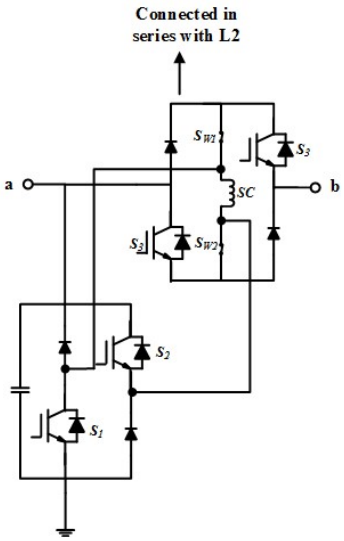

Fig. 11(b). The superconducting fault current limiter with superconducting magnetic energy storage with common superconductor.

4.3. Series dynamic braking resistor

A series Dynamic Braking Resistor (SDBR) can also be used to improve the FRT capability of the DFIG. The SDBR is placed in different locations and its impact has been evaluated. In [45], the SDBR is connected in series with the rotor. The rotor currents have been employed to trigger the SDBR and the active crowbar. The important advantage of the SDBR is to decrease the number of switching operation of the crowbar, which avoids the DFIG to operate as s squirrel cage induction generator during the fault condition. Furthermore, due to limiting the rotor over-current, the frequent performance of the DC braking chopper decreases. It means that the charging current of the DC link capacitor is reduced by the operation of the SDBR. It should be mentioned that the RSC switching stopped with the SDBR operation. Meanwhile, the SDBR in the rotor side decrease the rotor controllability.

In [46, 47], the SDBR is placed at the stator side of the DFIG. Its operation has been compared to the DC braking chopper operation. As discussed, the current control limiting devices in the stator side are effective for the voltage sag compensation. A summary of advantages and disadvantages of the fault current limiting devices are presented in Table I.

5. Simulation Results

In this section, the impact of the different locations and the type of impedance for the FCLs are studied. From the FCL's operation point of view, they should have very low impedance during normal condition, fast response after fault detection, high impedance value during the fault and also fast recovery time after fault removal. However, various configurations of the FCLs are a little bit different in the characteristics as mentioned above. For instance, regarding the configuration of the FCLs, some types of the FCLs are superconductive, then almost zero impedance in normal operation. Whilst for the other types, there is very small impedance. Meanwhile, the FCLs may have different response and recovery times considering their configurations.

Table I. A summary of characteristics of the fault current limiting devices

FCL type	Location	Impedance Type	Rotor Transient Over-Current Limitation	Stator Fault Current Limitation	Excess Active Power Evacuation	Terminal Voltage Sag Compensation	Rotor Switching State during the fault	Operation on Different Types of Fault	Components	SC.	Cost
SFCL-MES	L1 and L4	Inductive	L1: Yes (G.) L4: Yes (E.)	L1: Yes (E.) L4: Yes (G.)	No	L1: Yes (G.) L4: No	Continuous with different control, good controllability of the RSC in L1	Not effective in asymmetrical faults;	I-T*1 Diodes*6(CSC)*8(VSC) Inductor*1 S-S*0(CSC)*2(VSC)	Yes	High
Switch Type FCL	L1	Inductive	Yes (G.)	Yes (E.)	No	Yes (G.)	Continuous with good RSC controllability	Not effective in asymmetrical faults;	I-T*1 Diode*6 Inductor*1 S-S*1 A snubber circuit	No	Low
Active SFCL with Reactive Power Injection	L2	Inductive	Yes (G.)	Yes (E.)	No	Yes (G.)	Continuous with good RSC controllability	Effective for all fault types	I-T*1(superconductive) A low pass filter S-S*6 A split DC link capacitors	Yes	High
DC Resistive FCL	L2	Resistive	Yes (G.)	Yes (E.)	Yes	Yes (G.)	Continuous with good RSC controllability	Effective for all fault types	Diodes*12 SC*3	Yes	High
Resistive Flux Coupling Type SFCL	L1 and L4	Resistive	L1: Yes (E.) L4: Yes (G.)	L1: Yes (E.) L4: Yes (G.)	Yes	L1: Yes (G.) L4: No	Continuous with different control, good controllability of the RSC in L1	Effective for all fault types	Coupling Transformer*3 SC*3 S-S*3 Arrestor*3	Yes	High

Peer-reviewed version available at Appl. Sci. 2018, 8, 2059; doi:10.3390/app8112059

Resistive Type SFCL with SMES	L2	Resistive	Yes (G.)	Yes (E.)	Yes	Yes (E.)	Continuous with good RSC controllability	Effective for all fault types	Parallel Transformer*1 S-S*7 SC.*4 Diode*1 Capacitor*1	Yes	High
Resistive Type SFCL with Transient Voltage Control	L2	Resistive	Yes (G.)	Yes (E.)	Yes	Yes (E.)	Continuous with TVC, good controllability of the RSC	Effective for all fault types	SC.*3	Yes	High
Resistive Type SFCL, SMES with Common SC	L2	Resistive	Yes (G.)	Yes (E.)	Yes	Yes (E.)	Continuous with good RSC controllability	Effective for all fault types	S-S*18 SC.*3 Diode*12 Capacitor*3	Yes	High
Thyristor Bridge Type FCL with Bypass Resistor	L1	Resistive	Yes (G.)	Yes (E.)	Yes	Yes (E.)	Continuous with good RSC controllability	Not effective in asymmetrical faults;	I-T*1 Diode*1 Thyristor*6 Bypass resistor*3 Inductance*1	No	Low
Variable Resistive Type FCL	L2	Variable resistance	Yes (G.)	Yes (E.)	Yes, Controlled active power absorption	Yes (E.)	Continuous	Not effective in asymmetrical faults;	I-T*1 Diode*6 Inductor*1 S-S*1 Resistance*1	No	Low

Optimized Located FCL	L3	Resistive-Inductive	Yes (E.)	Yes (G.)	Yes, the rotor active power	No	Blocked	Effective for all fault types	S-S*2 Resistance*2 Inductance*2 Arrestor*2	No	Low
Non-controlled FCL	L1 and L4	Inductive	L1: Yes (G.) L4: Yes (E.)	L1: Yes (E.) L4: Yes (G.)	No	L1: Yes (G.) L4: No	Continuous	Effective for all fault types	I-T*1 Diode*6 Inductor*1	No	Low
Parallel Resonance Type FCL	L2	Resonance	Yes (G.)	Yes (E.)	Yes	Yes (E.)	Continuous	Effective for all fault types	S-S*3 Diode*15 Inductance*6 Capacitance*3	No	Low
SDBR	L1 and L4	Resistive	L1: Yes (G.) L4: Yes (E.)	L1: Yes (E.) L4: Yes (G.)	Yes	L1: Yes (G.) L4: No	Blocked	Effective for all fault types	Resistance*3 Thyristor*6	No	Low
I-T: Isolation Transformer; S-S: Semiconductor Switch; Li: Location no.; E.: Excellent; G.: Good; SC.: Superconductor;											

Peer-reviewed version available at Appl. Sci. 2018, 8, 2059; doi:10.3390/app8112059

However, it should be mentioned that after fault occurrence and during the fault steady state, all FCLs should have a high impedance value and only difference comes back to the impedance type. Therefore, the type of impedance and its impact on the operation of the DFIG and the FRT enhancement at three different locations including the stator side, the rotor side and the terminal side are taken into account. The DC link-location has the same effect of the rotor side location. So, in order to avoid proliferation, location 3 is not mentioned. The DFIG is connected to the grid through a three-phase transformer and a transmission line. The parameters of the simulation is presented in Table II. To have a reasonable comparison, the impedance values for the resistive and inductive type FCLs are the same. Meanwhile, to demonstrate how the FCL's impedance either as an inductive or a resistive could affect the RSC controllability, the impedance value is chosen regarding the FCL impact on the stator side. As discussed, the resistive type FCL in the stator side has a very effective operation because of voltage sag compensation, excess active power consumption and also increasing the RSC controllability. Therefore, the resistive type FCL in the stator side is selected as a reference to calculate the impedance value.

As it is mentioned, the different locations have different impacts on the FRT improvement of the DFIG. In this section, the rotor and stator currents are shown in Fig. 12.

Table II

Simulated DFIG Specifications

Rated Power	2MW	Rotor leakage inductance	0.12pu	DC bus capacitor	50mF
Rated Stator Voltage	690V	Magnetising Inductance	3.45pu	Resistance of grid side filter	0.3pu
Rated Frequency	60Hz	Stator to Rotor turns ratio	0.35	Reactance of grid side filter	0.003pu
Three phase transformer	0.69/34.5kV, 60Hz, 5MVA	Stator resistance	0.011pu	Nominal wind speed	13m/s
Transmission lines	30km, 0.01+j0.1Ω/km	Stator inductance	0.012pu	DC-chopper resistor	0.5 Ω
Stator leakage inductance	0.12pu	Rated DC-link voltage	1200V		

At first, the inductive type FCL is placed at three locations in the DFIG. The value of the inductance is less than the intersection point inductance value of the leakage coefficient curves as presented in Fig. 5(b). Then it can be concluded that the absolute value of the leakage coefficient for the inductive FCL in the rotor side is higher than for the inductive FCL in the stator side. As a result, with respect to the discussion in section IV-1-a, it is expected that the inductive FCL in the stator side or the rotor side or the terminal side has almost the same impact on the stator current. However, as it is predicted considering section IV-1-a, the rotor fault current level in the steady state of the fault for the inductive FCL in the rotor side is less than the other FCL locations due to high leakage coefficient value shown in Fig. 5(b).

In Fig. 12, the impact of the resistive type FCL for three locations are shown. As it is mentioned, the operation of the FCL with resistive impedance in the stator side is the most effective one in limiting both the stator and rotor currents level. The resistive impedance in the stator side is capable to

compensate the voltage sag in the DFIG terminal, and also to absorb excess active power during the fault conditions. For the FCL at the terminal side, its impact is almost the same when the FCL is in the stator side. By placing the FCL at the rotor side, due to decreasing the RSC controllability, there is a high current level in both the stator and rotor currents. However, in order to get good fault current limitation in the rotor side by the FCL, a high impedance value should be employed in the FCL either the inductive type FCL or the resistive type FCL.

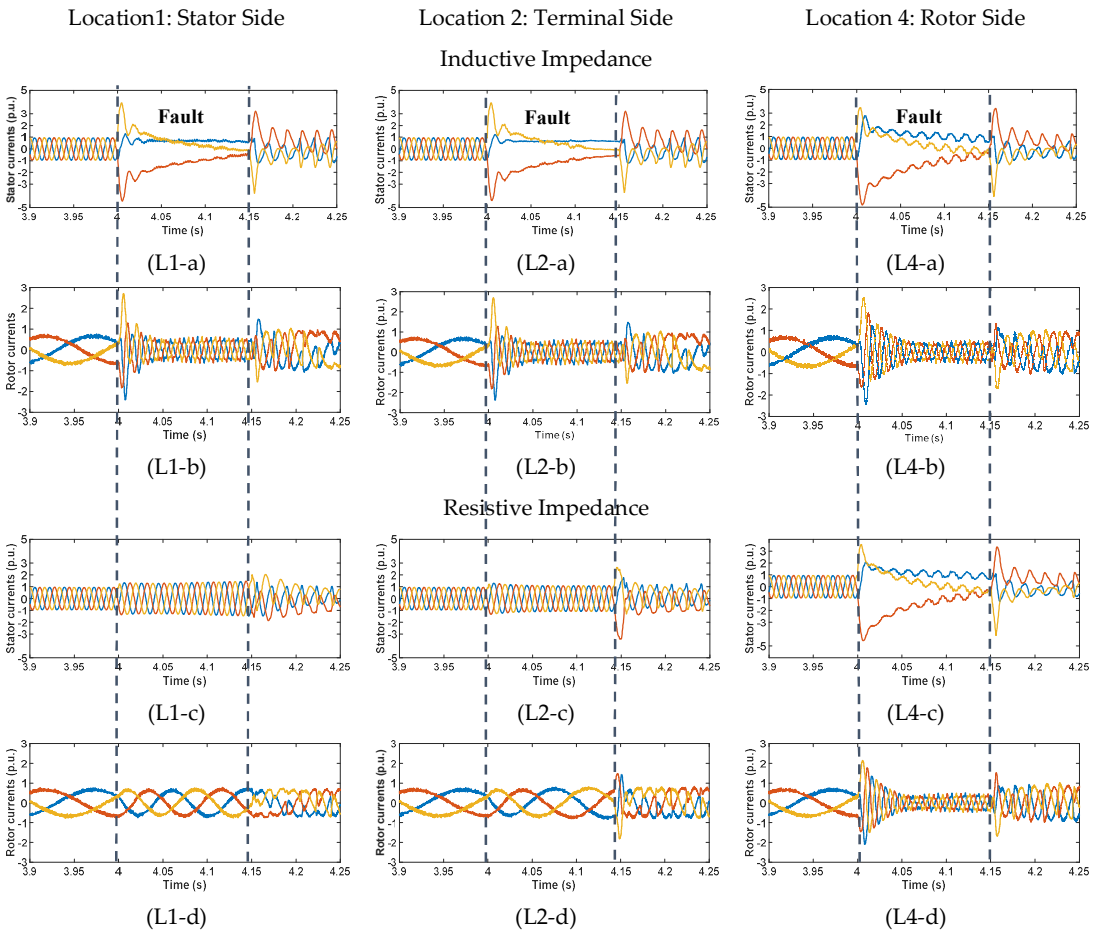

Fig. 12. Stator and rotor currents of the doubly fed induction generator during three-phase fault with the fault current limiter in the stator side L1, in the terminal side L2 and in the rotor side L4, the stator currents (a) with inductive fault current limiter and (c) with resistive fault current limiter. The rotor currents (b) with inductive fault current limiter and (d) with resistive fault current limiter.

6. Conclusion

In this paper, a review has been carried out on the FRT capability improvement of the DFIG by using fault current limiting devices. Almost, all types of the FCLs, which have been employed in the FRT of the DFIG, have been discussed. The operation of the FCLs have been explained regarding their locations in the DFIG and the impedance types. Three main locations including the stator side, the rotor side and the terminal side have been taken into account. Furthermore, for all these locations, the inductive and resistive type FCL have been placed and their impact on the terminal voltage sag compensation, the rotor and stator current limitation, excess active power consumption and the RSC controllability have been discussed. For the future works, in order to achieve a good fault current

Peer-reviewed version available at Appl. Sci. 2018, 8, 2059; doi:10.3390/app8112059

limitation with the FCL at the rotor side, the FCL should utilize high impedance value compared to the FCL located in the stator side. Meanwhile, with respect to the comparison, the best operation is granted to the resistive type FCL, which is located in the stator side, due to voltage sag compensation in the DFIG terminal, excess active power consumption and the RSC controllability increase.

Conflicts of Interest: The authors declare no conflict of interest.

References

1. M. Tsili and S. Papathanassiou, "A review of grid code technical requirements for wind farms," *IET Renewable Power Generation*, vol. 3, no. 3, pp. 308-332, 2009.
2. A. D. Hansen and G. Michalke, "Fault ride-through capability of DFIG wind turbines," *Renewable Energy*, vol. 32, no. 9, pp. 1594-1610, 2007.
3. J. LÓpez, E. GubÍa, P. Sanchis, X. Roboam, and L. Marroyo, "Wind Turbines Based on Doubly Fed Induction Generator Under Asymmetrical Voltage Dips," *IEEE Transactions on Energy Conversion*, vol. 23, no. 1, pp. 321-330, 2008.
4. K. Ma, *Power electronics for the next generation wind turbine system* vol. 5: Springer, 2015.
5. E. Netz, "Grid code; high and extra high voltage," *E. ON Netz GmbH, Bayreuth*, 2006.
6. J. J. Justo, F. Mwasilu, and J.-W. Jung, "Doubly-fed induction generator based wind turbines: A comprehensive review of fault ride-through strategies," *Renewable and Sustainable Energy Reviews*, vol. 45, pp. 447-467, 2015.
7. M. Q. Duong, G. N. Sava, F. Grimaccia, S. Leva, M. Mussetta, S. Costinas, *et al.*, "Improved LVRT based on coordination control of active crowbar and reactive power for doubly fed induction generators," in *Proc. 2015 9th International Symposium on Advanced Topics in Electrical Engineering (ATEE)*, 2015, pp. 650-655.
8. H. Ł, M. S. E. Moursi, and H. H. Zeineldin, "A Parallel Capacitor Control Strategy for Enhanced FRT Capability of DFIG," *IEEE Transactions on Sustainable Energy*, vol. 6, no. 2, pp. 303-312, 2015.
9. G. Pannell, B. Zahawi, D. J. Atkinson, and P. Missailidis, "Evaluation of the Performance of a DC-Link Brake Chopper as a DFIG Low-Voltage Fault-Ride-Through Device," *IEEE Transactions on Energy Conversion*, vol. 28, no. 3, pp. 535-542, 2013.
10. B. B. Ambati, P. Kanjiya, and V. Khadkikar, "A Low Component Count Series Voltage Compensation Scheme for DFIG WTs to Enhance Fault Ride-Through Capability," *IEEE Transactions on Energy Conversion*, vol. 30, no. 1, pp. 208-217, 2015.
11. P. S. Flannery and G. Venkataramanan, "Unbalanced Voltage Sag Ride-Through of a Doubly Fed Induction Generator Wind Turbine With Series Grid-Side Converter," *IEEE Transactions on Industry Applications*, vol. 45, no. 5, pp. 1879-1887, 2009.
12. H. Fathabadi, "Control of a DFIG-based wind energy conversion system operating under harmonically distorted unbalanced grid voltage along with nonsinusoidal rotor injection conditions," *Energy Conversion and Management*, vol. 84, no. 8, pp. 60-72, 2014.
13. J. Lopez, P. Sanchis, X. Roboam, and L. Marroyo, "Dynamic Behavior of the Doubly Fed Induction Generator During Three-Phase Voltage Dips," *IEEE Transactions on Energy Conversion*, vol. 22, no. 3, pp. 709-717, 2007.
14. W. Guo, L. Xiao, S. Dai, Y. Li, X. Xu, W. Zhou, *et al.*, "LVRT Capability Enhancement of DFIG With Switch-Type Fault Current Limiter," *IEEE Transactions on Industrial Electronics*, vol. 62, no. 1, pp. 332-342, 2015.
15. S. H. Hosseini, M. B. B. Sharifian, and F. Shahnia, "Dynamic performance of double fed induction generator for wind turbines," in *Proc. 2005 International Conference on Electrical Machines and Systems*, 2005, pp. 1261-1266 Vol. 2.

16. D. Xie, Z. Xu, L. Yang, J. Østergaard, Y. Xue, and K. P. Wong, "A Comprehensive LVRT Control Strategy for DFIG Wind Turbines With Enhanced Reactive Power Support," *IEEE Transactions on Power Systems,* vol. 28, no. 3, pp. 3302-3310, 2013.
17. M. Rahimi and M. Parniani, "Efficient control scheme of wind turbines with doubly fed induction generators for low-voltage ride-through capability enhancement," *IET Renewable Power Generation,* vol. 4, no. 3, pp. 242-252, 2010.
18. P. Kanjiya, B. B. Ambati, and V. Khadkikar, "A Novel Fault-Tolerant DFIG-Based Wind Energy Conversion System for Seamless Operation During Grid Faults," *IEEE Transactions on Power Systems,* vol. 29, no. 3, pp. 1296-1305, 2014.
19. P. S. Flannery and G. Venkataramanan, "A Fault Tolerant Doubly Fed Induction Generator Wind Turbine Using a Parallel Grid Side Rectifier and Series Grid Side Converter," *IEEE Transactions on Power Electronics,* vol. 23, no. 3, pp. 1126-1135, 2008.
20. W. Qiao, R. G. Harley, and G. K. Venayagamoorthy, "Coordinated Reactive Power Control of a Large Wind Farm and a STATCOM Using Heuristic Dynamic Programming," *IEEE Transactions on Energy Conversion,* vol. 24, no. 2, pp. 493-503, 2009.
21. W. Qiao, R. G. Harley, and G. K. Venayagamoorthy, "Effects of FACTS Devices on a Power System Which Includes a Large Wind Farm," in *Proc. 2006 IEEE PES Power Systems Conference and Exposition*, 2006, pp. 2070-2076.
22. A. O. Ibrahim, T. H. Nguyen, D. C. Lee, and S. C. Kim, "A Fault Ride-Through Technique of DFIG Wind Turbine Systems Using Dynamic Voltage Restorers," *IEEE Transactions on Energy Conversion,* vol. 26, no. 3, pp. 871-882, 2011.
23. M. T. Hagh, S. B. Naderi, and M. Jafari, "Application of Non-superconducting Fault Current Limiter to improve transient stability," in *Proc. 2010 IEEE International Conference on Power and Energy*, 2010, pp. 646-650.
24. S. B. Naderi, M. Negnevitsky, A. Jalilian, M. T. Hagh, and K. M. Muttaqi, "Optimum Resistive Type Fault Current Limiter: An Efficient Solution to Achieve Maximum Fault Ride-Through Capability of Fixed-Speed Wind Turbines During Symmetrical and Asymmetrical Grid Faults," *IEEE Transactions on Industry Applications,* vol. 53, no. 1, pp. 538-548, 2017.
25. M. Jafari, S. B. Naderi, M. T. Hagh, M. Abapour, and S. H. Hosseini, "Voltage Sag Compensation of Point of Common Coupling (PCC) Using Fault Current Limiter," *IEEE Transactions on Power Delivery,* vol. 26, no. 4, pp. 2638-2646, 2011.
26. S. B. Nderi, M. Negnevistky, A. Jalilian, and M. T. Hagh, "Non-controlled fault current limiter to improve fault ride through capability of DFIG-based wind turbine," in *Proc. 2016 IEEE Power and Energy Society General Meeting (PESGM)*, 2016, pp. 1-5.
27. M. Mardani and S. H. Fathi, "Fault current limiting in a wind power plant equipped with a DFIG using the interface converter and an optimized located FCL," in *Proc. The 6th Power Electronics, Drive Systems & Technologies Conference (PEDSTC2015)*, 2015, pp. 328-333.
28. W. Guo, L. Xiao, S. Dai, X. Xu, Y. Li, and Y. Wang, "Evaluation of the Performance of BTFCLs for Enhancing LVRT Capability of DFIG," *IEEE Transactions on Power Electronics,* vol. 30, no. 7, pp. 3623-3637, 2015.
29. M. K. Hossain and M. H. Ali, "Transient Stability Augmentation of PV/DFIG/SG-Based Hybrid Power System by Nonlinear Control-Based Variable Resistive FCL," *IEEE Transactions on Sustainable Energy,* vol. 6, no. 4, pp. 1638-1649, 2015.

30. S. B. Naderi, M. Jafari, and M. Tarafdar Hagh, "Controllable resistive type fault current limiter (CR-FCL) with frequency and pulse duty-cycle," *International Journal of Electrical Power & Energy Systems,* vol. 61, no. 10, pp. 11-19, 2014.
31. G. Rashid and M. H. Ali, "Application of parallel resonance fault current limiter for fault ride through capability augmentation of DFIG based wind farm," in *Proc. 2016 IEEE/PES Transmission and Distribution Conference and Exposition (T&D)*, 2016, pp. 1-5.
32. S. B. Naderi, M. Jafari, and M. T. Hagh, "Parallel-Resonance-Type Fault Current Limiter," *IEEE Transactions on Industrial Electronics,* vol. 60, no. 7, pp. 2538-2546, 2013.
33. W. Guo, L. Xiao, and S. Dai, "Enhancing Low-Voltage Ride-Through Capability and Smoothing Output Power of DFIG With a Superconducting Fault-Current Limiter Magnetic Energy Storage System," *IEEE Transactions on Energy Conversion,* vol. 27, no. 2, pp. 277-295, 2012.
34. W. Guo, L. Xiao, and S. Dai, "Fault current limiter-battery energy storage system for the doubly-fed induction generator: analysis and experimental verification," *IET Generation, Transmission & Distribution,* vol. 10, no. 3, pp. 653-660, 2016.
35. L. Chen, F. Zheng, C. Deng, Z. Li, and F. Guo, "Fault Ride-Through Capability Improvement of DFIG-Based Wind Turbine by Employing a Voltage-Compensation-Type Active SFCL," *Canadian Journal of Electrical and Computer Engineering,* vol. 38, no. 2, pp. 132-142, 2015.
36. M. M. Hossain and M. H. Ali, "Transient stability improvement of doubly fed induction generator based variable speed wind generator using DC resistive fault current limiter," *IET Renewable Power Generation,* vol. 10, no. 2, pp. 150-157, 2016.
37. M. Hossain and H. Ali, "Asymmetric fault ride through capability enhancement of DFIG based variable speed wind generator by DC resistive fault current limiter," in *Proc. 2016 IEEE/PES Transmission and Distribution Conference and Exposition (T&D)*, 2016, pp. 1-5.
38. L. Chen, C. Deng, F. Zheng, S. Li, Y. Liu, and Y. Liao, "Fault Ride-Through Capability Enhancement of DFIG-Based Wind Turbine With a Flux-Coupling-Type SFCL Employed at Different Locations," *IEEE Transactions on Applied Superconductivity,* vol. 25, no. 3, pp. 1-5, 2015.
39. R. Ou, X. Y. Xiao, Z. C. Zou, Y. Zhang, and Y. H. Wang, "Cooperative Control of SFCL and Reactive Power for Improving the Transient Voltage Stability of Grid-Connected Wind Farm With DFIGs," *IEEE Transactions on Applied Superconductivity,* vol. 26, no. 7, pp. 1-6, 2016.
40. I. Ngamroo and T. Karaipoom, "Cooperative Control of SFCL and SMES for Enhancing Fault Ride Through Capability and Smoothing Power Fluctuation of DFIG Wind Farm," *IEEE Transactions on Applied Superconductivity,* vol. 24, no. 5, pp. 1-4, 2014.
41. I. Ngamroo and T. Karaipoom, "Improving Low-Voltage Ride-Through Performance and Alleviating Power Fluctuation of DFIG Wind Turbine in DC Microgrid by Optimal SMES With Fault Current Limiting Function," *IEEE Transactions on Applied Superconductivity,* vol. 24, no. 5, pp. 1-5, 2014.
42. Z. C. Zou, X. Y. Chen, C. S. Li, X. Y. Xiao, and Y. Zhang, "Conceptual Design and Evaluation of a Resistive-Type SFCL for Efficient Fault Ride Through in a DFIG," *IEEE Transactions on Applied Superconductivity,* vol. 26, no. 1, pp. 1-9, 2016.
43. Z. C. Zou, X. Y. Xiao, Y. F. Liu, Y. Zhang, and Y. H. Wang, "Integrated Protection of DFIG-Based Wind Turbine With a Resistive-Type SFCL Under Symmetrical and Asymmetrical Faults," *IEEE Transactions on Applied Superconductivity,* vol. 26, no. 7, pp. 1-5, 2016.
44. J. Mohammadi, S. Afsharnia, S. Vaez-Zadeh, and S. Farhangi, "Improved fault ride through strategy for doubly fed induction generator based wind turbines under both symmetrical and asymmetrical grid faults," *IET Renewable Power Generation,* vol. 10, no. 8, pp. 1114-1122, 2016.

45. J. Yang, J. E. Fletcher, and J. O'Reilly, "A Series-Dynamic-Resistor-Based Converter Protection Scheme for Doubly-Fed Induction Generator During Various Fault Conditions," *IEEE Transactions on Energy Conversion,* vol. 25, no. 2, pp. 422-432, 2010.
46. K. E. Okedu, "Enhancing DFIG wind turbine during three-phase fault using parallel interleaved converters and dynamic resistor," *IET Renewable Power Generation,* vol. 10, no. 8, pp. 1211-1219, 2016.
47. K. E. Okedu, S. M. Muyeen, R. Takahashi, and J. Tamura, "Wind Farms Fault Ride Through Using DFIG With New Protection Scheme," *IEEE Transactions on Sustainable Energy,* vol. 3, no. 2, pp. 242-254, 2012.